Numerical and experimental insights into acoustic emission from a train wheelset

L. Taenzer, D. Tallarico, A. Kandiah, B. Van Damme, A. Bergamini
Empa - Swiss Federal Laboratories for Material Science and Technology,
Laboratory for Acoustics/ Noise Control ,
Ueberlandstrasse 129, 8600 Dübendorf, Switzerland
e-mail: **linus.taenzer@empa.ch**

Abstract
Structural vibrations of railway components such as wheels and rails are the main cause of noise emission. In this work, we investigate both numerically and experimentally, the structural vibrations and sound emission from a train wheelset under lab-conditions. The main focus is on the investigation of sound propagation in the fluid domain considering three alternative acoustic sources structural boundary values are projected upon: the analytical model of a discretized circular disk mounted to an infinite rigid baffle using the discrete calculation method (DCM), a closed cylinder volume using the boundary element method (BEM) and a cylinder in a cubic enclosure using the finite element method (FEM). We put a special emphasis on calculating the impedance matrix that connects sound pressures and normal velocities obtained from the structural analysis at the vibrating wheel. In view of future acoustics, reflections from a sound-hard surface are taken into account using the half-space Green's function.

1 Introduction

The noise emission of railway traffic is still a major research topic. Railway noise is caused by fluid-dynamic effects, structure borne sound and electric machines such as transformers and cooling systems. Rolling noise contributes considerably to the overall sound emissions and is dominant for train speeds between 30 and 250 km/h [1]. The wheel-rail interaction is often considered by its subcomponents in order to examine their share more closely [2]. There are several ways to reduce noise which can be, for example limited operational speed, protection barriers [3], or optimization of components which strongly emit noise such as the wheel [4]. To deal with public requirements and regulations and collecting data cheaply and fast, there is an increasing need for detailed physics-based models of noise emission for each separate subcomponent. Furthermore, they provide the possibility to investigate different effects such as wheel flats [5], contact areas and polygonization [6].
Sound emission from train wheel sets has been modelled via a plethora of analytical (simplified models [7]) and numerical (finite element and BEM [8], [5]) techniques. With the boundary element method, complex geometries can be investigated, but also precise meshes for a closed surfaces are needed. One simple model which is customary in building acoustics but has not been investigated in railway wheel emission is the model of a piston mounted on a baffle, which is generally only used for uniform velocities. However, several authors developed expressions for a discretized vibrating piston with non-uniform velocity using analytical solutions [9] or asymptotic expressions for calculating the mutual impedance between the rectangular [10] or circular [11] discretized elements of the oscillating plate. A precise formulation of the impedance of a discretized plate is published in [12] also referred to as the Discrete Calculation Method (DCM). To the best of our knowledge, there is no work available, comparing DCM for the acoustic impedance connecting acoustic pressure and structural velocity. Most works considering DCM method investigate the overall radiation efficiency in the far field such as e.g. [13]. The goal of this work is to show that the DCM and in particular the predicted impedance matrix can be used to reduce the computational effort and simplify the entire model significantly by

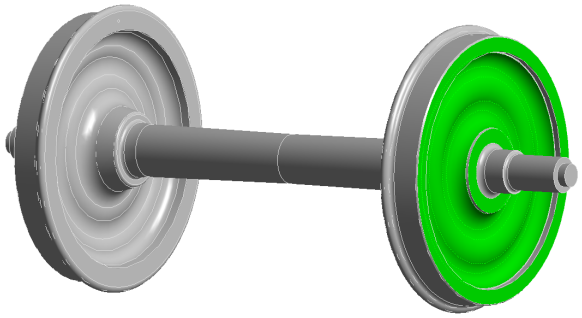

Figure 1: 3D model of railway wheelset.

- considering sound waves in the far-field and
- provided that radiation from the edges is negligible.

For the acoustic source, surface velocity input data of the vibrating structure is generally taken from harmonic finite element analysis. It is a common tool for characterizing railway wheels [14] that can be used for noise reduction shape optimization [15].
In this work, we study both numerically and experimentally the structural vibrations and sound emission from a train wheelset with free boundary conditions. The modeling of sound propagation in the fluid domain follows a boundary element method approach. We put a special emphasis on calculating the impedance matrix that relates sound pressure and normal velocities at the vibrating wheelset. The impedance matrix can be obtained using different approaches, such as the combined Helmholtz integral equation formulation in the boundary element method and the discrete calculation method (DCM). The two methods take into account near-field and far-field assumptions, respectively. As a third numerical model for acoustic noise emission, we use a more standard FE method in the acoustic domain. We highlight the computational benefit of the BEM methods compared to the FE method for problems involving free-field emission of sound.

2 Theory

2.1 Harmonic analysis

In the finite element harmonic analysis, the railway wheel is excited by a unit force F parallel to the axle and at a specific node and the mode shapes $\mathbf{u}$ are obtained by solving the equation of motion

$$\left(-\omega^2 M + j\omega C + K\right)\mathbf{u} = F, \tag{1}$$

where $\mathbf{F}$ is now a nodal vector. The quantities are defined in appendix A. The normal velocities on the front surface (green area in Fig. 1) are extracted with $\mathbf{v}_n = 2\pi f \mathbf{u}_n$. The wheel is excited at one specific node over all frequencies and the displacements $\mathbf{u}$ are calculated using the finite element method in Ansys.

2.2 Acoustic analysis

The data from the harmonic analysis is used to develop a model for the noise radiation. The output normal velocities $\mathbf{v}_n$ are used as input data and projected onto a flat surface. In the first step, the equation

$$\mathbf{p_s} = Z\mathbf{v_n} \tag{2}$$

is needed to calculate the impedance matrix Z of the surface in order to obtain the surface pressure $\mathbf{p}_s$ from the input normal velocity $\mathbf{v}_n$. In the following, three methods are used in order to calculate the acoustic impedance whose governing equations are summarized in Tab. 1.

Table 1: Expressions of the acoustic impedance matrix Z and associated literature.

	Impedance Z	Author
Baffled piston with DCM	$z_{ii} = \rho c \left[1 - \frac{J_1(2ka)}{ka} + \frac{S1(2ka)}{ka}\right]$ $z_{ij} = j\rho ckaA_i \frac{e^{-jkab}}{2\pi b} \left[\frac{2J_1(ka)}{ka} \frac{2J_1(kad)}{kad}\right]$	[12]
Boundary element method	$Z = [C - A]^{-1} B$	[16]
Fluid structure interaction	$Z = -[-\omega^2 M_F + j\omega C_F + K_F]^{-1}(j\omega\rho_0 R_f)$	[17]

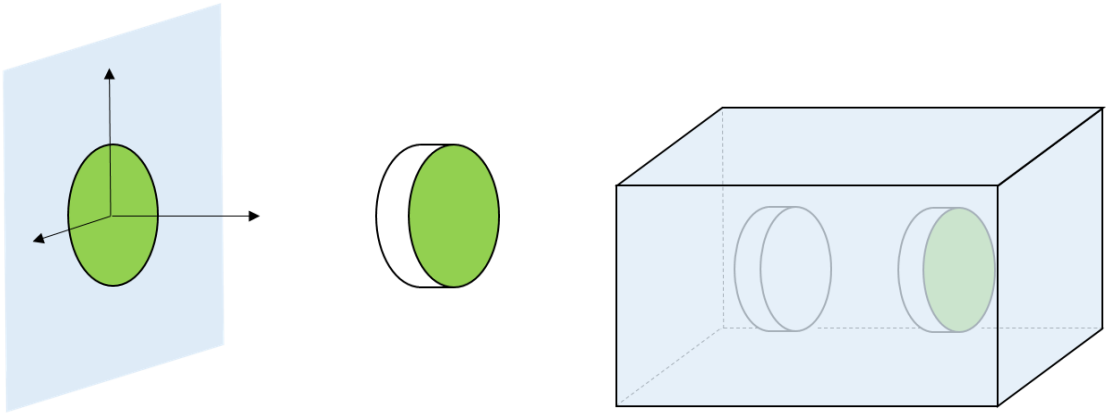

(a) Circular piston mounted on an infinite rigid baffle. (b) Closed surface for boundary element method. (c) Finite element model with enclosure for fluid domain.

Figure 2: Models for noise propagation

The three different emission models are illustrated in Fig. 2. Illustration 2a shows a circular piston mounted on an infinite rigid baffle, 2b, a cylinder with a closed surface used in the boundary element method and 2c, two cylinders surrounding the wheels of the original wheelset in a cubic enclosure, which approximates the fluid domain using the finite element method. To calculate the pressure over the wheel's surface from its normal vibration velocity, all three methods perform the computations of the impedance relation. Following that, the noise propagation is calculated, using the Green's function for models 2a and 2b, whereas for the finite element method the pressure distribution is solved for all degrees of freedom in the discretized volume. The baffle is the computationally least expensive method since one needs to simply calculate the pressure values on the disk and a set of selected receiver points. The cylinder is computationally more expensive since one needs to calculate the pressures on two circular areas and the lateral area. The finite element model is the computationally most expensive method since the entire volume around the cylinders is discretized and contributing to the solution in the selected receiver points.

2.2.1 Discretization of a baffled piston

At first, we look at a circular disk mounted on an infinite rigid baffle, see Fig. 2a. In this setup with constant surface velocity, an analytical far field solution exists [18] which can be written as

$$p(r,\theta,ka) = jka\rho c\left\{\frac{2J_1(ka\,sin(\theta))}{(ka\,sin(\theta))}\right\}\frac{e^{-jkar}}{2r}v. \tag{3}$$

Since the velocities over the wheel are not homogenous, the system is discretized in many little disks which behave again like baffled pistons. The impedance is split up in the self radiation impedance

$$z_{ii} = \rho c\left[1 - \frac{J_1(2ka)}{ka} + \frac{S_1(2ka)}{ka}\right] \tag{4}$$

and the mutual radiation impedance

$$z_{ij} = j\rho ckas_i\frac{e^{-jkab}}{2\pi b}\left[\frac{2J_1(ka)}{ka}\frac{2J_1(kad)}{kad}\right] \tag{5}$$

as reported in [12]. It is called the Discrete Calculation Method (DCM), which is limited to the far field and neglecting edge effects causing scattering.

2.2.2 Boundary element method

The analytically more complex method is the boundary element method which takes radiation effects of edges and therefore the more realistic boundary conditions into account, see Fig. 2b. In [16], the authors use the combined Helmholtz integral equation formulation (CHIEF) so that more complex geometries with complex meshes can be treated and the uniqueness problem is solved by introducing additional points, leading to an over-determined system that is solvable. Generally, the impedance on the surface is solved by discretizing the Kirchhoff-Helmholtz integral leading to the discretized equation

$$C\mathbf{p}_s = A\mathbf{p}_s - B\mathbf{v}_s, \tag{6}$$

where $A_{ij} = G(r_i, r_j)s_i$ and $B_{ij} = j\omega\rho\frac{\partial G(r_i,r_j)}{\partial n}s_i$ where G is the Green's function and i and j are the elements on the vibrating surface. r_i and r_j are the spatial coordinates of the disk's center position and s_i is the surface area which is the same for all elements. $C(x)$ is interior 1 and exterior 0. On the surface itself it is the geometric quantity of the surface angle, which is generally 0.5 for continuous surfaces.

From Eq. 6, the impedance matrix becomes

$$Z = -(C - A)^{-1}B. \tag{7}$$

As described in [19] the expression for the Green's function is

$$G(x,y) = \frac{e^{jkR}}{4\pi R} + R_I\frac{e^{jkR'}}{4\pi R'}. \tag{8}$$

where $R_I = 0$ for an infinite space and $R_I = 1$ for a semi-infinite hard-boundary space.
$R = \sqrt{(x-x_s)^2 + (y-y_s)^2 + (z-z_s)^2}$ and $R' = \sqrt{(x-x_s)^2 + (y-y_s)^2 + (z+z_s)^2}$ are the distances between receiver and the source and receiver and the image source respectively with the receiver position $r = (x, y, z)$ and source at position $r_s = (x_s, y_s, z_s)$, only valid if the reflecting plane is the xy plane. The half space assumption is equivalent to a mirrored, virtual second source leading to the hard boundary condition of

$$\mathbf{v}(\mathbf{r}_{rp})\mathbf{n}_{rp} = 0, \tag{9}$$

which considers normal velocities equal to zero at the reflecting plane with coordinates $\mathbf{r}_{rp}$ and normal vector $\mathbf{n}_{rp}$.

2.2.3 Finite element method

For one-way coupling of a fluid-structure interaction problem in the frequency domain the impedance matrix is calculated with the matrices obtained from the discretisation in the finite element domain. It is described as

$$Z = -[-\omega^2 M_F + j\omega C_F + K_F]^{-1}(j\omega\rho_0 R_f) \tag{10}$$

with M_f, C_f, and K_f being the mass, damping and stiffness matrix of the fluid, and the coupling matrix R_f importing the displacements of selected nodes from the harmonic analysis [17].

3 Results

3.1 Structural vibrational analysis

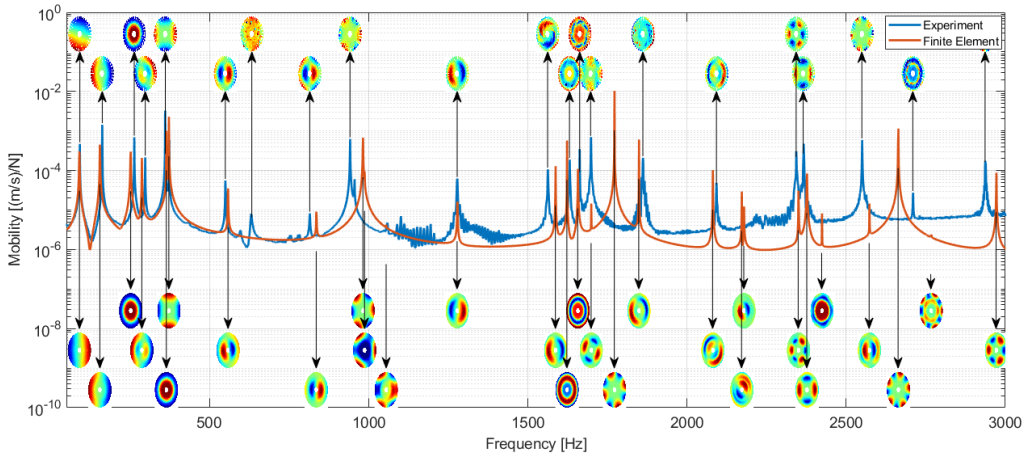

Figure 3: Mobility of the velocity per unit force in axial direction with visualized mode shapes at frequency peaks.

To validate the results from the time harmonic FEA, the numerical predictions are compared to the laservibrometer measurements. The wheel DB97 is excited in axial direction with a shaker as a mechanical excitation source and a laser vibrometer is used to measure the velocities in axial direction. The wheel has a radius of 0.45 meter and a weight of around 1000 kg. In Fig. 3 , the comparison between the harmonic FEM model and the measurements in axial direction are shown. The model is investigated under free conditions, implemented by laying the wheelset axle on a wooden support equipped with rubber pads. Both the frequencies and their absolute values agree very well between experiment and simulation. The mode shapes are shown at several frequency peaks.

3.2 Acoustic emission

The described models in 2.2 are realized with different software tools. The DCM model is programmed in Matlab. The BEM model is realized by using the OpenBEM code developed by [16] and the finite element model is built in Ansys [17].

3.2.1 Pressure on input surface obtained by impedance

The three models are compared by evaluating the pressures on a line at the surface of the wheel as shown in Fig. 4a. The green area represents the surface where the fluid-structure interaction occurs (contributions

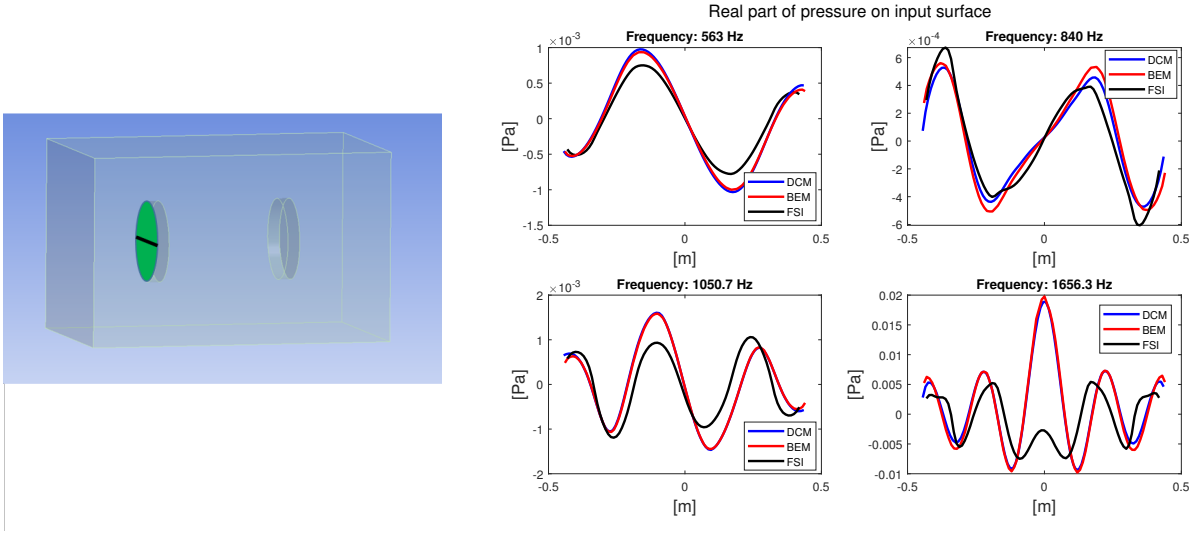

(a) Schematic view of evaluated surface. (b) Pressures distribution evaluated at selected modes.

Figure 4: Evaluation of pressure modes on input surface.

from the axle and other surfaces are assumed negligible to the frontal emission of the single wheel). The impedance matrix Z is evaluated to obtain the surface pressure p_s from the normal velocities v_n. Since a comparison of the impedance matrix between the different methods is not possible due to different meshes (triangular elements for Open BEM, tetrahedrons for FSI and quadrilateral for the DCM method), the pressure distribution along the marked line is shown for selected modes, see Fig. 4b. The pressures between the baffled piston and the boundary element are in very good agreement, while the finite element model gives more divergent results, which is well known in research as the enclosure in a finite volume faces several difficulties such as boundary conditions at infinity (in our case we use absorption boundaries in Ansys) and mesh size of the elements, which limits the range of valid frequencies, in our case from 200-2000 Hz.

3.2.2 Pressure on receiver surface

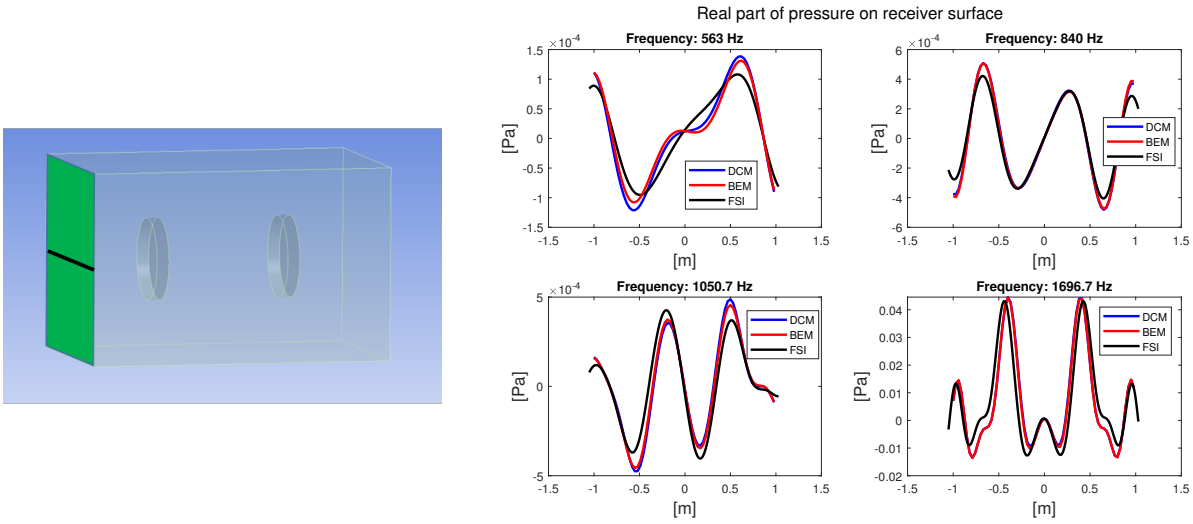

(a) Schematic view of evaluated surface. (b) Pressures distribution evaluated at selected modes.

Figure 5: Pressures compared at surface 0.88 meters away from wheel.

In order to evaluate the pressures away from the surface, the distance of 0.88 meters is selected. This is mainly dictated by computational feasibility of the FE model: the enclosure must be large enough to absorb outgoing waves properly and small enough so that computational feasibility is still guaranteed. This means that for the valid frequency range, the distance of the absorption boundary must be at least half the wavelength away from the source and the elements of the air must be meshed at least with 6 elements per wavelength to avoid numerical instability using linear shape functions. The modes are evaluated at the black line in Fig. 5a and show very good agreement even for the finite element method in Fig 5b.

3.2.3 Ground effects

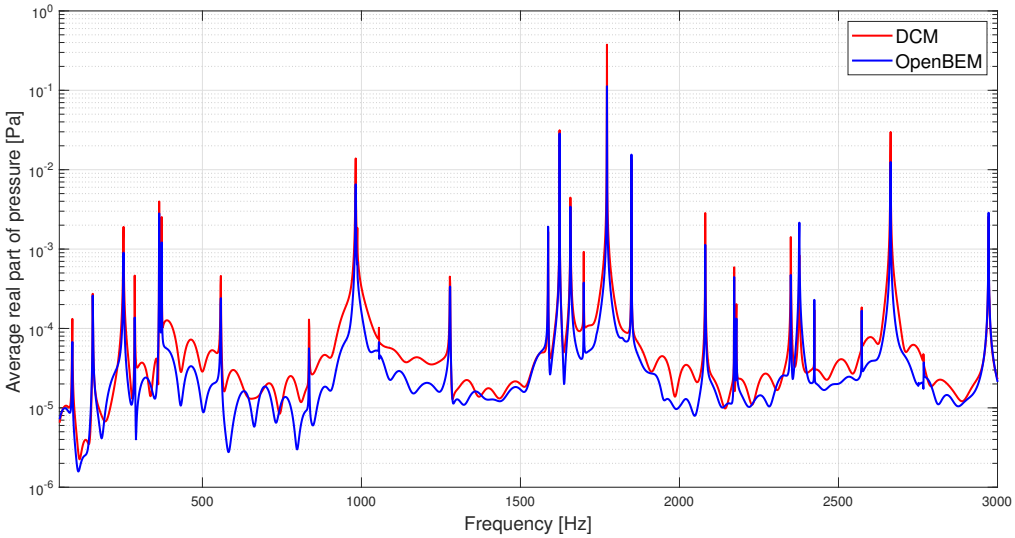

Figure 6: Frequency response of averaged microphones at height of 1.5 meter.

As a final step, ground effects are included by running the calculation with half-space assumption. We consider points on a line 2 meters away and in a height of 1.5 meters. They are spaced equally every 10 cm from -0.8 to 0.8 meters along that line. The averaged value over the number of points per frequency is displayed for each method in Fig. 6. This shows that the peaks (both magnitude and frequency) are well captured by the simulation models.

The comparison can be seen more closely when looking at single modes not only along a line but on an entire surface at 2 meters distance away with a width of 2.1 meters and a height of 1.9 meters, see Fig. 7. Three resonance frequencies are selected and the occurring mode shapes are compared. Although the difference in magnitude is varying, it is possible to clearly identify the modes visually for DCM and BEM.

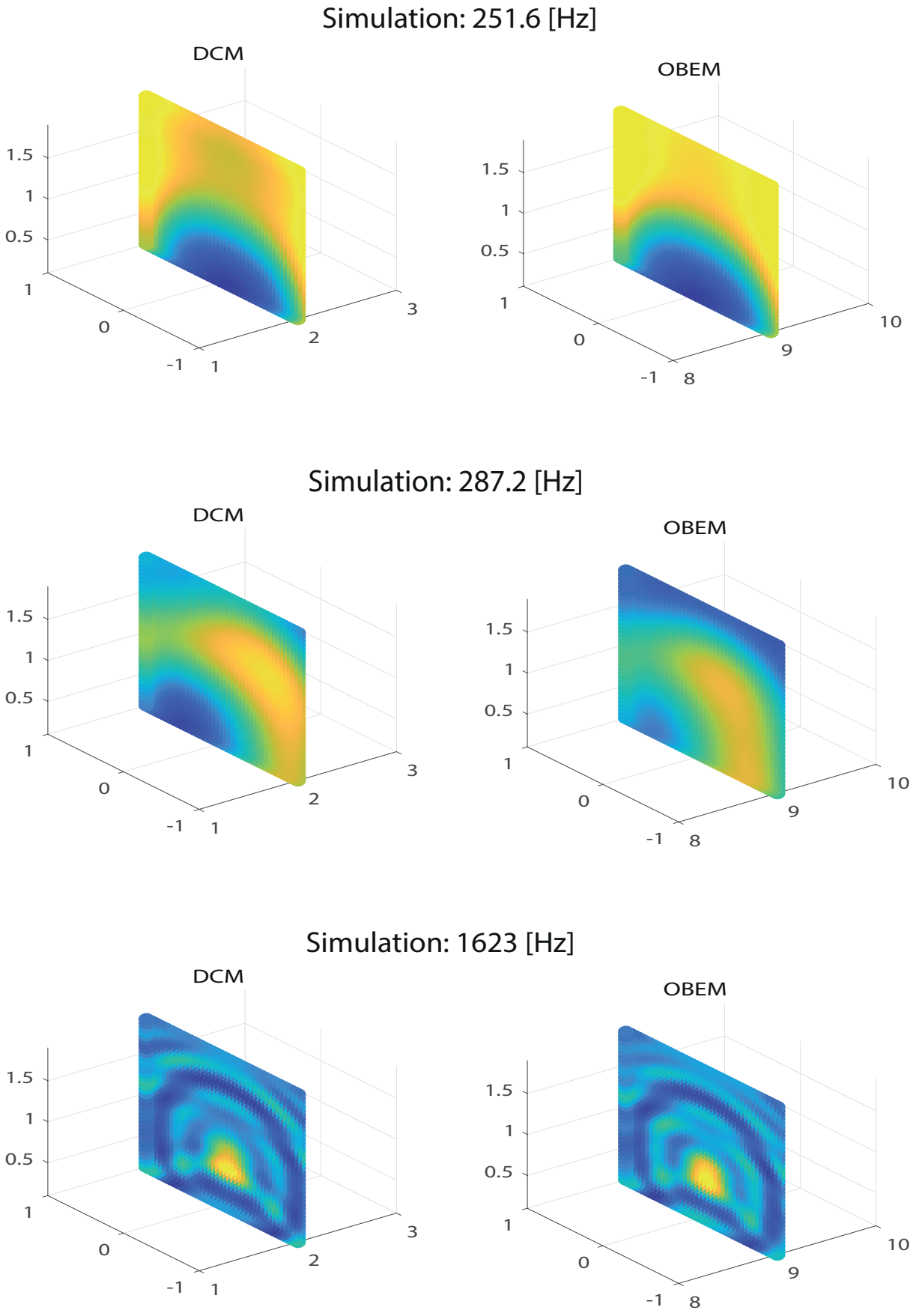

Figure 7: Comparison of simulated sound radiation pattern of three different wheel vibration modes.

3.3 Computational effort and limitations

Comparing the three models, the model with the baffled piston is the least computationally expensive. Only a single circular plane is discretized into square elements, so fewer elements are needed. Also, no additional computational effort is required for surfaces and normal vectors, since all elements have the same size and orientation. On the other hand, the boundary element model generally considers closed volumes and approximates more complex geometries with triangular meshes, which more than doubles the number of discretized surface elements and requires detailed calculations of surface properties such as the normal vector and area of each element. This allows the use of more complex geometries, but significantly increases the computational cost. From a computational viewpoint, the finite element method is the most computationally intensive method. The entire volume must be discretized, and far-field calculations become difficult as the number of elements increases considerably. For high frequencies, the mesh size must be at least six linear elements per wavelength, making calculations over a large frequency spectrum of 50-6000 Hz impractical.

4 Conclusion

We have studied the vibrometric behaviour and acoustic emission of a train wheelset. Detailed investigation of the three mathematical models showed that the model of a vibrating disk mounted on an infinite rigid baffle gives results comparable to the OpenBEM code. Fluid-structure interaction in finite elements, on the other hand, is very time consuming. Boundary conditions and mesh size require a large volume range to be valid for the entire frequency range from 50 to 2000 Hz. The computational cost is about 50 hours compared to 5 hours for the baffle piston approach. However the limitation of the baffled piston is alleviated by the fact that a wheelset is very thick at the edges and thus effectively baffled. In future work, the accurate emission models will be compared to experiments.

Acknowledgments

The project was commissioned and funded by the Swiss Confederation. (contract number 1337000438).

References

[1] D. Jeong, H. S. Choi, Y. J. Choi, and W. Jeong, "Measuring Acoustic Roughness of a Longitudinal Railhead Profile Using a Multi-Sensor Integration Technique," *Sensors 2019, Vol. 19, Page 1610*, vol. 19, no. 7, p. 1610, apr 2019. [Online]. Available: https://www.mdpi.com/1424-8220/19/7/1610/htmhttps://www.mdpi.com/1424-8220/19/7/1610

[2] D. Thompson, "Railway Noise and Vibration," *Railway Noise and Vibration*, 2009.

[3] C. Talotte, P. E. Gautier, D. J. Thompson, and C. Hanson, "Identification, modelling and reduction potential of railway noise sources: a critical survey," *Journal of Sound and Vibration*, vol. 267, no. 3, pp. 447–468, oct 2003.

[4] J. Gutiérrez-Gil, X. Garcia-Andrés, J. Martínez-Casas, E. Nadal, and F. D. Denia, "Mitigation of Railway Wheel Rolling Noise by Using Advanced Optimization Techniques," *EngOpt 2018 Proceedings of the 6th International Conference on Engineering Optimization*, pp. 1141–1153, 2019. [Online]. Available: https://link.springer.com/chapter/10.1007/978-3-319-97773-7_99

[5] K. Cui and X. Qin, "Numerical computation of wheel-rail impact noises with considering wheel flats based on the boundary element method," *Journal of Vibroengineering*, vol. 18, no. 6, pp. 3930–3940, sep 2016. [Online]. Available: https://www.extrica.com/article/16804https://www.extrica.com/article/16804/abs

[6] K. Liu and L. Jing, "A finite element analysis-based study on the dynamic wheel–rail contact behaviour caused by wheel polygonization:," *https://doi.org/10.1177/0954409719891549*, vol. 234, no. 10, pp. 1285–1298, dec 2019. [Online]. Available: https://journals.sagepub.com/doi/abs/10.1177/0954409719891549

[7] P. J. Remington, "Wheel/rail noise- Part I: Characterization of the wheel/rail dynamic system," *Journal of Sound and Vibration*, vol. 46, no. 3, pp. 359–379, jun 1976.

[8] T. Zhong, G. Chen, X. Sheng, X. Zhan, L. Zhou, and J. Kai, "Vibration and sound radiation of a rotating train wheel subject to a vertical harmonic wheel–rail force," *Journal of Modern Transportation*, vol. 2, no. 26, pp. 81–95, jun 2018. [Online]. Available: https://www.infona.pl//resource/bwmeta1.element.springer-doi-10_1007-S40534-017-0154-6

[9] R. L. Pritchard, "Mutual Acoustic Impedance between Radiators in an Infinite Rigid Plane," *Citation: The Journal of the Acoustical Society of America*, vol. 32, p. 730, 1960. [Online]. Available: https://doi.org/10.1121/1.1908199

[10] E. M. Arase, "Mutual Radiation Impedance of Square and Rectangular Pistons in a Rigid Infinite Baffle," *Citation: The Journal of the Acoustical Society of America*, vol. 36, p. 1521, 1964. [Online]. Available: https://doi.org/10.1121/1.1919236

[11] P. R. Stepanishen, "Evaluation of mutual radiation impedances between circular pistons by impulse response and asymptotic methods," *Journal of Sound and Vibration*, vol. 59, no. 2, pp. 221–235, jul 1978.

[12] N. Hashimoto, "Measurement of sound radiation efficiency by the discrete calculation method," *Applied Acoustics*, vol. 62, no. 4, pp. 429–446, apr 2001.

[13] K. Kolber, A. Snakowska, and M. Kozupa, "The effect of plate discretization on accuracy of the sound radiation efficiency measurements," *Archives of Acoustics*, vol. 39, no. 4, pp. 511–518, 2014.

[14] A. Cigada, S. Manzoni, and M. Vanali, "Vibro-acoustic characterization of railway wheels," *Applied Acoustics*, vol. 69, no. 6, pp. 530–545, jun 2008.

[15] X. Garcia-Andrés, J. Gutiérrez-Gil, J. Martínez-Casas, and F. D. Denia, "Wheel shape optimization approaches to reduce railway rolling noise," *Structural and Multidisciplinary Optimization*, vol. 62, no. 5, pp. 2555–2570, nov 2020. [Online]. Available: https://link.springer.com/article/10.1007/s00158-020-02700-6

[16] V. Cutanda Henríquez and P. M. Juhl, "OpenBEM-An open source Boundary Element Method software in Acoustics," 2010, pp. 1–10. [Online]. Available: www.octave.org

[17] I. Ansys, *Theory Reference Ansys*, release 20 ed., 2022.

[18] D. T. Blackstock and A. A. Atchley, *Fundamentals of Physical Acoustics*. Wiley, 2000.

[19] H. Brick and M. Ochmann, "A half-space BEM for the simulation of sound propagation above an impedance plane," *The Journal of the Acoustical Society of America*, vol. 123, no. 5, p. 3418, may 2008. [Online]. Available: https://asa.scitation.org/doi/abs/10.1121/1.2934160

Appendix

A Nomenclature

s_i	Cross-sectional area of a discretized piston element
k	Wave number
ρ	Density
J_1	Bessel function of the first kind
S_1	Struve function of the first kind
c	Speed of sound
j	Imaginary number
ω	Angular frequency
M	Mass matrix
K	Stiffness matrix
D	Damping matrix
u	Structural displacement
F	Force
v_n	Normal velocity
v_s	Source velocity
f	Frequency
p_s	Surface pressure
Z	Acoustic impedance matrix
G	Green's function
a	Disk radius
M_f	Mass matrix of fluid
K_f	Stiffness matrix of fluid
D_f	Damping matrix of fluid
R_f	Coupling matrix between solid and fluid DOF